Sevenfold- and sixfold-coordinated Zr^{3+} ions in cubic stabilized zirconia: Crystal-field approach

C. B. Azzoni and A. Paleari
Dipartimento di Fisica "A. Volta" dell'Università di Pavia, via Bassi 6, I-27100, Pavia, Italy
(Received 29 January 1991; revised manuscript received 2 April 1991)

Crystal-field calculations of the energy structure of the 4*d* multiplet of the Zr^{3+} ion were carried out for a large number of configurations of the environment in the crystal lattice of cubic stabilized zirconia, starting from neutron-diffraction data. The presence of oxygen vacancies gives rise to sixfold- and sevenfold-coordinated sites where the crystal field is strongly distorted with respect to regular crystal sites and cannot be treated with the perturbative approximation of weak distortions. The problem of the assignment of the axial EPR signal and of the optical-absorption bands to sixfold- and sevenfold-coordinated sites is discussed.

I. INTRODUCTION

It is well known that x-ray irradiation and thermochemical reduction of yttria-stabilized zirconia (YSZ) give rise to paramagnetic centers associated with the oxygen vacancies which are included in the cubic structure of the crystal:[1] In fact this is constituted by a cationic sublattice of Zr^{4+} ions and substitutional Y^{3+} ions, and by an anionic sublattice which is locally disordered by the rearrangements of the oxygen positions around the vacancies. During both types of treatment, electrons are released in the material and then trapped near the positively charged oxygen vacancies. We will distinguish between two types of electronic trapping which give rise to paramagnetic defects: "anionic," if the electron is in oxygen vacancy; "cationic," if the electron is in a cationic site near an oxygen vacancy. In the first case the defect is F^+-center-like, while in the second case it consists of a cation with a trapped 4*d* electron.

At least three distinct types of paramagnetic defects have been identified with use of electron paramagnetic resonance (EPR) spectroscopy. Three models have so far been proposed for one of these which is characterized by an axial structure: an anionic model (F^+),[2] an extrinsic cationic model (Ti^{3+}),[3,4] and an intrinsic cationic one (Zr^{3+}).[5,6] This variety of proposals clashes with a well defined experimental signal with precise features: (a) axial anisotropy of the g tensor with $g_\parallel = 1.98$ and $g_\perp = 1.85$; (b) multiplicity of the EPR spectrum: four equivalent sites exist in the crystal lattice, with the defect axis parallel to one of the four crystal directions $\langle 111 \rangle$; (c) anisotropy of the linewidth which varies with π periodicity between 0.7 mT (when the magnetic field **B** is parallel to the $\langle 111 \rangle$ crystal axis) and about 6 mT (when $\mathbf{B} \perp \langle 111 \rangle$); (d) asymmetry of the signal, evident in conditions of minimum linewidth; and (e) absence of hyperfine structures, particularly structures due to interactions between the electronic spin of the defect ($S = \frac{1}{2}$) and the nuclear spin of the yttrium ions (100% $I = \frac{1}{2}$). The origin of the axial features of the signal is the symmetry of the environment of nearest neighbors: in the case of a cationic defect the axial symmetry in the $\langle 111 \rangle$ direction may be due to a rearrangement of the nearest-neighboring oxygens caused by the presence of oxygen vacancies, while, for an anionic F^+-like defect, the cause of the observed axiality should be looked for in an asymmetry of the tetrahedron of nearest-neighboring cations around the vacancy, then in the presence of substitional Y^{3+} ions. Indeed, the anionic defect model has been abandoned for the absence of hyperfine structures from yttrium nuclei and for the too low values of the principal components of g tensor with respect to the free electron value $g_e = 2.0023$. On the other hand, the cationic defect model Ti^{3+} clashes with the experimental evidence that no type of impurity has ever been found in YSZ with a concentration consistent with the measured paramagnetic defect density (up to 0.1 mol %). For these reasons we proposed a model of intrinsic defect consisting of an electron trapped in a 4*d* orbital of a Zr^{3+} ion in a crystal field heavily modified with respect to the cubic field of an unperturbed site of the perfect lattice.[5] From this model it is possible, among other things, to give an explanation of the observed anisotropy of the EPR signal linewidth: Situations are indeed known in the literature where a $4d^1$ ion is in an orbitally nondegenerate ground state giving $g_\parallel \simeq 2 > g_\perp$ and where the $\Delta g_\perp = g_e - g_\perp$ shift depends on the ratio between the spin-orbit coupling constant λ and the crystal-field splitting:[7] Thus, the variations from site to site of the crystal field mainly affect the $g_\perp$ value giving rise to a $g_\perp$-value distribution which results in a linewidth anisotropy with π periodicity.[5]

Since we lacked indications suggesting the detailed structure of the defect, we originally proposed that it may consist in a Zr^{3+} ion coordinated with seven oxygens in presence of a vacancy.[5] Subsequently, other authors[6] proposed a model constituted by a Zr^{3+} ion coordinated with six oxygens in presence of two vacancies, instead of one, at the opposite corners of the cube of nearest neighbors around the central cation. These authors assert that the sevenfold-coordinated sites, statistically more abundant than the sixfold-coordinated ones, cannot give an EPR signal, being assimilable with ion site in a cubic field of a trigonally distorted eightfold coordination, which therefore have an orbitally degenerate ground state.

Really, also in this case the defect may give an observable EPR signal. But this and all the other speculations about the defect were lacking of any theoretical analysis of the energy level configuration of the possible EPR center structures.

In order to obtain a more detailed picture of the defect structure and to verify the preliminary proposals, we performed an *ab initio* crystal-field calculation from which it results that the Zr^{3+} ion in the presence of oxygen vacancies is really subjected to a strongly distorted crystal field: it is therefore impossible to obtain reliable results for this system on the basis of standard perturbative calculations like those referred to weak trigonal distortion of a regular cubic structure. Our calculations confirm the validity of the particular mechanism of anisotropic signal broadening we have already proposed taking into account the disordered rearrangement of oxygen sublattice due to the presence of vacancies. The results allow us to discriminate the sixfold- and sevenfold-coordinated sites and, moreover, a relation is suggested between optical properties and differently coordinated Zr^{3+} sites.

II. CRYSTAL-FIELD APPROACH

Owing to the mainly ionic nature of the Zr—O bond,[8] a crystal-field approach seems reasonably applicable. The electrostatic potential on the $4d^1$ electron of zirconium, with spatial coordinate $\mathbf{r}$, is determined by the charges q_j at the positions $\mathbf{R}_j$ of the surrounding ions considered as point-like charges. In the expression $V(\mathbf{r})=\sum_j q_j/|(\mathbf{R}_j-\mathbf{r})|$ the sum may be limited, in a good approximation, to the next nearest neighboring ions, then the $(8-n)$ oxygen ions coordinated with the Zr^{3+} ion, where n is the number of oxygen vacancies in the defect. In order to calculate $V(\mathbf{r})$, we use the following form of the potential:

$$V(\mathbf{r})=\sum_n \sum_m \sum_j \frac{4\pi}{2n+1} q_j \frac{r^n}{R^{n+1}} Z_{nm}^{c/s}(\mathbf{R}_j) Z_{nm}^{c/s}(\mathbf{r}) , \tag{1}$$

where the expansion in n terms with the tesseral harmonics $Z_{nm}^{c/s}$ is based on the expansion of $1/|(\mathbf{R}-\mathbf{r})|$ using the Legendre polynomials. This expansion is limited to the terms with $n=0,2,4$ because the potential acts on a d-like electron within the $4d$ multiplet[9] (admixture with s, p, or f orbitals is neglected). Other generic constrictions on the m index or s (sin) and c (cos) type of functions, which are related to the particular symmetry of the system, have been avoided in order to treat the problem more generally. For all the configurations analyzed the terms

$$c_{nm}^{c/s}=\sum_j \left[\frac{4\pi}{2n+1}\right] q_j Z_{nm}^{s/c}(\mathbf{r}_j)/R_j^{n+1}$$

have been calculated in function of the anionic coordinates to obtain the expression of the Hamiltonian $\mathcal{H}_{CF}$ with the Stevens's equivalent operators $\mathcal{O}_{nm}^{s/c}$:

$$\mathcal{H}_{nm}=\sum_{n,m} F_{nm}^{s/c}\mathcal{O}_{nm}^{s/c} \quad \text{with} \quad F_{nm}^{s/c}=a_{nm}^{s/c}c_{nm}^{c/s}\vartheta_n\langle r^n\rangle , \tag{2}$$

where $a_{nm}^{s/c}$ are the numerical factors which multiply the Cartesian functions $f_{nm}^{s/c}$ in the expression $Z_{nm}^{s/c}=a_{nm}^{s/c}f_{nm}^{s/c}(x,y,z)/r^n$, ϑ_n are the Stevens's multiplicative factors and $\langle r^n\rangle$ is the expectation value of r^n for the wave function of the Zr^{3+} $4d^1$ electron. The coefficients $F_{nm}^{s/c}$ of the Stevens's operators weight the different types of operators in the Hamiltonian, depending on the system symmetry. For low symmetry and without a center of inversion, all the $F_{nm}^{s/c}$, for $n=0,2,4$, may differ from zero. We emphasize that the separation of the terms of cubic symmetry from the low-symmetry ones, as in a perturbative approach, is not possible here, because the ionic displacements are considerable: The presence of anionic vacancies in the cube of nearest neighbors of the paramagnetic ions forces the oxygen relative positions to rearrange by about 15% compared to the unperturbed cubic ones. In fact the configurations analyzed are based on crystallographic data, particularly neutron-diffraction measurements,[10] which indicate that the presence of oxygen vacancies causes oxygen ions displacements $\epsilon\simeq 0.14a/2$ along the $\langle 100\rangle$ directions, with respect to the perfect lattice positions. Here $a\simeq 5.14$ Å is the lattice parameter and $a/2$ the edge of the unperturbed cube of anions around the zirconium ion.

In the case of sevenfold-coordinated Zr^{3+} we have considered a cube of nearest-neighboring ions where the displacements of the ions near the vacancy [oxygens 1, 2, and 3 in Fig. 1(a)] are directed towards the vacancy, the ion opposite to the vacancy [oxygen 7 in Fig. 1(a)] may move along any one of the three edges starting from its corner, while the other three oxygens [numbered 4, 5, and 6 in Fig. 1(a)] move towards one of the two neighboring ions near the vacancy. These constrictions determine 24 possible sevenfold-coordinated configurations. Other sevenfold-coordinations have been considered for which the oxygen opposite to the vacancy moves along the edges of adjacent cells [see Fig. 1(b)]. We have also analyzed simplified sevenfold-coordinated configurations not based on neutron-diffraction data but with oxygen dis-

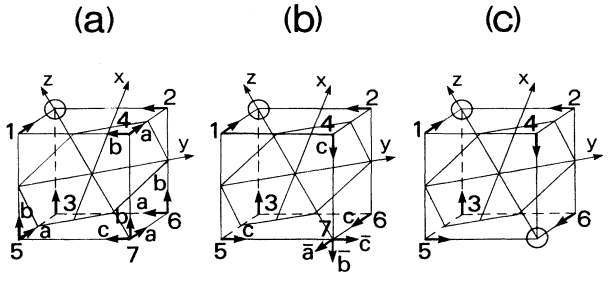

FIG. 1. Positions of the oxygen ions in the cube of nearest neighbors of an (a),(b) sevenfold- and (c) sixfold-coordinated Zr^{3+} ion. The oxygen vacancy sites are indicated by open circles and the oxygen rearrangements around the vacancies by arrows starting from the regular lattice positions. Oxygen sites and displacements are numbered and labeled, respectively, referring to Table I.

placements which keep the trigonal symmetry suggested by the experimental data. These configurations include one with the seven oxygens at the corners of the regular cube of nearest neighbors, one where the only three neighbors of the vacancy move towards it, one where all the oxygens of the cell except that opposite to the vacancy move towards it (three along the edges and three along the face diagonals of the cube), and, finally, one with six oxygens as in Fig. 1(c), showing a sixfold coordination, with a seventh oxygen at one of the two vacancy sites. These symmetric sevenfold coordinations will be referred to as 7sym(A), 7sym(B), 7sym(C), and 7sym(D), respectively.

On the other hand, in the case of sixfold-coordinated Zr^{3+}, the presence of two oxygen vacancies on the body diagonal of the cube restricts the possible anionic rearrangements to the symmetric one where the nearest neighbors of the vacancies move along the edges towards the nearest vacancy [see Fig. 1(c)].

All the data we present in the next section are referred to a Cartesian reference frame with $z\|[111]$, $x\|[\bar{1}\,\bar{1}2]$, and $y\|[1\bar{1}0]$. The eigenstates and the eigenvalues of the Zr^{3+} ion have been calculated diagonalizing the Hamiltonian

$$\mathcal{H}=\mathcal{H}_{\rm CF}+\mathcal{H}_{\rm s.o.}=-|e|V(\mathbf{r})+\lambda\mathbf{L}\cdot\mathbf{S}\ , \tag{3}$$

assuming the spin-orbit coupling constant equal to 250 cm^{-1}, rather than the free ion value 500 cm^{-1}, to take into account the strong reduction of orbital moment in oxides.[6,11] The g tensor is obtained by applying the Zeeman Hamiltonian $\mathcal{H}_Z=\mu_0(\mathbf{L}+2\mathbf{S})\cdot\mathbf{H}$ to the ground state when it is a Kramer doublet.

III. RESULTS

We started studying the possible crystal fields of the Zr^{3+} site by analyzing the results obtained by binding direction and magnitude of the oxygen displacements to the neutron-diffraction data. The crystal fields of the sevenfold-coordinated configurations determined by the 24 combinations of displacements of Fig. 1(a) cause, as main effect, the complete breaking of the 4d multiplet of the Zr^{3+} ion with a total energy splitting of about 3.5 eV and energy separation between the two lowest states ranging from 0.13 to 1.28 eV (see Table I). Indeed the anionic displacements are considerable and their possible combinations give rise to crystal fields of low symmetry, as the values of the Stevens's coefficients clearly indicate.

TABLE I. Energy-level splittings (eV) of the 4d orbitals of Zr^{3+} in the crystal field of seven oxygens displaced from the vertices of the cube of nearest neighbors as shown in Figs. 1(a) and 1(b), and assuming $\lambda=250$ cm^{-1}. In the column of configuration the combinations of displacements of the oxygens are indicated following the same labeling as Fig. 1. The energy difference between the ground state and the first excited one is reported in the last column.

n	Configuration	Energy levels of 4d multiplet					Δ_{max}	δ
1	(4a 5a 6a 7a)	1.91	1.08	−0.58	−0.93	−1.58	3.49	0.65
2	(4b 5a 6a 7a)	1.86	1.16	−0.51	−1.24	−1.37	3.23	0.13
3	(4a 5b 6a 7a)	1.61	1.29	−0.43	−1.12	−1.46	3.07	0.34
4	(4b 5b 6a 7a)	1.67	1.24	−0.33	−1.19	−1.49	3.16	0.30
5	(4a 5a 6b 7a)	1.95	1.00	−0.54	−1.04	−1.47	3.42	0.43
6	(4b 5a 6b 7a)	1.61	1.29	−0.43	−1.12	−1.46	3.07	0.34
7	(4a 5b 6b 7a)	2.06	0.88	−0.48	−0.64	−1.92	3.98	1.28
8	(4b 5b 6b 7a)	2.01	0.90	−0.22	−0.87	−1.92	3.93	1.05
9	(4a 5a 6a 7b)	1.68	1.23	−0.31	−1.25	−1.46	3.14	0.21
10	(4b 5a 6a 7b)	1.68	1.22	−0.31	−1.25	−1.45	3.13	0.20
11	(4a 5b 6a 7b)	1.51	1.35	−0.48	−1.19	−1.36	2.87	0.17
12	(4b 5b 6a 7b)	1.74	1.15	−0.45	−1.15	−1.40	3.14	0.25
13	(4a 5a 6b 7b)	1.74	1.15	−0.45	−1.15	−1.40	3.14	0.25
14	(4b 5a 6b 7b)	1.51	1.35	−0.42	−1.19	−1.36	2.87	0.17
15	(4a 5b 6b 7b)	1.83	1.12	−0.51	−0.97	−1.58	3.41	0.61
16	(4b 5b 6b 7b)	1.83	1.12	−0.51	−0.97	−1.58	3.41	0.61
17	(4a 5a 6a 7c)	1.74	1.28	−0.52	−0.96	−1.65	3.39	0.69
18	(4b 5a 6a 7c)	1.91	1.09	−0.58	−0.93	−1.59	3.50	0.66
19	(4a 5b 6a 7c)	1.61	1.30	−0.43	−1.11	−1.46	3.07	0.35
20	(4b 5b 6a 7c)	1.95	1.00	−0.54	−1.03	−1.47	3.42	0.44
21	(4a 5a 6b 7c)	1.66	1.24	−0.33	−1.18	−1.49	3.15	0.31
22	(4b 5a 6b 7c)	1.61	1.30	−0.43	−1.12	−1.46	3.07	0.34
23	(4a 5b 6b 7c)	2.01	0.90	−0.23	−0.88	−1.90	3.91	1.02
24	(4b 5b 6b 7c)	2.06	0.88	−0.48	−0.65	−1.90	3.96	1.25
25	(4c 5c 6c 7$\bar{a}$)	1.75	1.58	−0.91	−1.10	−1.18	2.93	0.08
26	(4c 5c 6c 7$\bar{b}$)	1.75	1.58	−0.90	−1.10	−1.19	2.94	0.09
27	(4c 5c 6c 7$\bar{c}$)	1.75	1.58	−0.91	−1.10	−1.18	2.93	0.08

TABLE II. Principal g values and angles between the defect Z axis and the (111) crystal direction, for the sevenfold-coordinated configurations of Table I, assuming $\lambda=250\ cm^{-1}$.

N	g_Z	g_X	g_Y	ϑ_Z
1	1.950	1.804	1.969	0.5
2	1.736	2.087	1.577	4.2
3	1.946	1.879	1.894	2.2
4	1.949	1.858	1.875	4.4
5	1.942	1.870	1.896	1.5
6	1.951	1.857	1.910	2.8
7	1.960	1.979	1.868	0.0
8	1.960	1.980	1.812	0.5
9	1.933	1.673	1.954	3.6
10	1.912	1.670	1.940	1.8
11	1.920	1.945	1.812	3.0
12	1.938	1.919	1.831	1.2
13	1.938	1.919	1.831	1.2
14	1.922	1.947	1.820	2.3
15	1.959	1.971	1.803	2.3
16	1.959	1.971	1.803	2.3
17	1.957	1.818	1.964	1.1
18	1.952	1.801	1.969	0.6
19	2.630	0.735	0.744	21.0
20	1.943	1.863	1.903	1.0
21	1.942	1.847	1.879	1.3
22	1.944	1.872	1.901	1.9
23	1.960	1.979	1.865	0.3
24	1.956	1.980	1.868	0.1

The g values for these configurations are shown in Table II: The different combinations of oxygen displacements generate a wide range of g_X and g_Y values, while, except for a few cases, the g_Z value does not change very much from a configuration to another and the Z axis of the defect lies in directions not far from the $\langle 111 \rangle$ crystal axis. The g values vary within the experimental range, but in no case is the symmetry of the g tensor axial and most axial configurations (where $g_X \simeq g_Y$) do not possess any preferential feature. But, it is to be noted, there is no particular reason why these sevenfold-coordinated configurations, if they exist, do not give an EPR signal.

The sevenfold-coordinated configurations of Fig. 1(b), where the oxygen opposite to the vacancy rearranges along the edges of the adjacent cube of the anion sublattice, also show the complete breaking of the $4d^1$ multiplet but they give an orbital ground state which lies fairly close to other orbital states which may cause very efficient spin-lattice relaxation effects (also owing to the high spin-orbit coupling constant of the Zr^{3+} ion), making the observation of the magnetic resonance practically impossible. At the bottom of Table I, the eigenvalues for these configurations are given. The eigenvalues of the symmetric sevenfold-coordinated configurations 7sym($A-D$), obtained by relaxing the constraints on the oxygen displacements suggested by the neutron-diffraction data, are shown in Table III. In these cases the orbital ground state is practically degenerate and it consists of the slightly perturbed cubit orbital doublet Γ_3.

The simplest sixfold-coordinated configuration, consistent with the neutron-diffraction data, is that of Fig. 1(c). The strong trigonal distortion due to the two oxygen vacancies forces the orbital state $|0\rangle$ at the ground state, giving a perfectly axial ground state with the axis along the $\langle 111 \rangle$ crystal direction. In Table IV the eigenvalues and eigenstates of the $4d$ multiplet are shown. It is to be noted that the first excited level derives from the orbital doublet Γ_3. The calculated values of the g tensor are $g_\parallel=1.995$ and $g_\perp=1.815$. We observe a good agreement with the experimental values within the approximation of the crystal-field approach, which takes into account covalent effects only through an empirical lowering of the λ value. It should be noted that the expressions of the eigenstates and the value of $\Delta g_\perp$ are different from those given in literature in the case of an octahedron with a weak trigonal distortion. From the calculated g values we deduce $g_\perp \simeq 2-5\lambda/\delta$, against the expression $g_\perp=2-2\lambda/\delta$ valid for a $4d^1$ ion in a weakly trigonal distorted octahedron, and used by Orera *et al.*,[6] which leads to a wrong estimate of the energy δ starting from the experimental g values.

IV. DISCUSSION

From our results it is possible to draw attention to some features of the Zr^{3+} site which are independent of the exact configuration of the defect. As we have already proposed, the disordered rearrangement of the oxygen sublattice seems mainly to affect the orthogonal components of the g tensor with respect to the defect axis which deviates from the $\langle 111 \rangle$ direction of the cubic structure with a certain angular distribution. Moreover, the calculation of the energy levels for all the configurations considered gives unexpected splittings of the $4d$ multiplet. In order to discuss the features of these splittings, the energy-level structures in cubal and octahedral crystal fields are compared in Table V with simple cases of sixfold and sevenfold coordinations with the

TABLE III. Energy-level splittings (eV) of the $4d$ orbitals of Zr^{3+} in sevenfold-coordination ($\lambda=250\ cm^{-1}$) with symmetric oxygen displacements (see text). Δ_{max} is the total splitting and δ the energy difference between the ground state and the first excited one.

n	Configuration	Energy levels of $4d$ multiplet					Δ_{max}	δ
28	[7sym(A)]	1.64	1.60	−0.54	−1.43	−1.44	3.08	0.01
29	[7sym(B)]	1.28	1.25	−0.58	−0.98	−0.98	2.26	0.00
30	[7sym(C)]	2.22	2.17	−1.12	−1.73	−1.75	3.93	0.02
31	[7sym(D)]	1.44	1.42	−0.24	−1.28	−1.29	2.73	0.01

TABLE IV. Energy levels and wave functions for the $4d$ multiplet of Zr^{3+} in the sixfold-coordinated configuration of Fig. 1(c) with $\lambda=250\ cm^{-1}$.

E (eV)	Eigenstates
+1.993	$0.54\cdot\|-1,+\frac{1}{2}\rangle+0.01\cdot\|0,-\frac{1}{2}\rangle-0.84\cdot\|2,+\frac{1}{2}\rangle$ $0.84\cdot\|-2,-\frac{1}{2}\rangle+0.01\cdot\|0,+\frac{1}{2}\rangle+0.54\cdot\|1,-\frac{1}{2}\rangle$
+1.959	$0.83\cdot\|-2,+\frac{1}{2}\rangle+0.55\cdot\|1,+\frac{1}{2}\rangle+0.02\cdot\|2,-\frac{1}{2}\rangle$ $-0.02\cdot\|-2,+\frac{1}{2}\rangle-0.55\cdot\|-1,-\frac{1}{2}\rangle+0.83\cdot\|2,-\frac{1}{2}\rangle$
−0.995	$0.01\cdot\|-2,+\frac{1}{2}\rangle-0.83\cdot\|-1,-\frac{1}{2}\rangle-0.55\cdot\|2,-\frac{1}{2}\rangle$ $-0.55\cdot\|-2,+\frac{1}{2}\rangle+0.83\cdot\|1,+\frac{1}{2}\rangle-0.01\cdot\|2,-\frac{1}{2}\rangle$
−0.996	$0.54\cdot\|-2,-\frac{1}{2}\rangle-0.04\cdot\|0,+\frac{1}{2}\rangle-0.84\cdot\|1,-\frac{1}{2}\rangle$ $-0.84\cdot\|-1,+\frac{1}{2}\rangle-0.04\cdot\|0,-\frac{1}{2}\rangle-0.54\cdot\|2,+\frac{1}{2}\rangle$
−1.780	$-0.02\cdot\|-2,-\frac{1}{2}\rangle-0.999\cdot\|0,+\frac{1}{2}\rangle+0.04\cdot\|1,-\frac{1}{2}\rangle$ $0.04\cdot\|-1,+\frac{1}{2}\rangle-0.999\cdot\|0,-\frac{1}{2}\rangle+0.02\cdot\|2,+\frac{1}{2}\rangle$

anions at the regular corners of the cube of nearest neighbors, while the effects of the oxygen opposite to the vacancy in the sevenfold coordination are investigated moving it along the $\langle 111\rangle$ direction. Consideration of these situations leads to the following points.

(a) The simplified sixfold-coordinated configuration has an energy structure [Table V($D1$)] which well reproduces the main features of the more realistic situation of Table IV and which seems to derive from a cubal field structure [Table V($A1,2$)] except for the state $|0\rangle$ which lies at the lowest energy. This leads to a trigonal EPR signal and to a shift $\Delta g_\perp=5.5\lambda/\delta$ different from $2\lambda/\delta$ for the presence of the Γ_3 orbital doublet as first excited states instead of the doublet coming from the Γ_5 manifold as in octahedral field [Table V($B2$)].

(b) The regular sevenfold-coordination [Table V($C1$)] gives a splitting similar to the cubal field one, but the state $|0\rangle$ lies just above the degenerate orbital doublet Γ_3. By removing the oxygen opposite the vacancy along the $\langle 111\rangle$ direction, the orbital singlet $|0\rangle$ is pushed below the doublet [Table V($C2$)], but the inversion of the energy levels is reached for displacements of the oxygen larger than about 0.5 Å which is of the same order of magnitude as the real ionic displacements in the oxygen sublattice.

(c) From (a) and (b) it results that the energy-level structure of both the sevenfold- and sixfold-coordinated Zr^{3+} are similar to that of a cubal field, but with the state $|0\rangle$ at lower energy. Really the lowering of the orbital singlet $|0\rangle$ appears to be the main effect of the strong trigonal field generated by the presence of oxygen vacancies into the defect.

In contrast with the situations of Table V, which do not take into account the oxygen displacements deduced from diffraction measurements, the realistic configurations of Tables I and IV show more complex admixtures of states but the same qualitative features. In particular (i) the sixfold-coordinated configuration of Fig. 1(c) gives results in good agreement with the experimental data; (ii) many of the sevenfold-coordinated configurations (see Table II) should give an EPR signal with g values about 1.9 but without the axial symmetry along the $\langle 111\rangle$ directions and, for this reason, it is unlikely that they exist; (iii) sevenfold-coordinated sites in more symmetric configurations, as those of Table III, possess energy structures similar to that in Table V($C1$) with the orbital doublet Γ_3 as ground state: such a ground state, whose degeneracy may be removed by Jahn-Teller effect,[12] has not the required symmetry and would give an EPR signal actually not observed; (iv)

TABLE V. Energy-level structure of the $4d$ multiplet of Zr^{3+} in (1) regular and (2) weakly trigonally distorted (A) cubal and (B) octahedral environments, compared with ($C1$) the sevenfold and ($D1$) the sixfold coordinations of Fig. 1 neglecting ionic displacements from the regular lattice sites. In ($C2$) the oxygen opposite to the vacancy is removed along the $\langle 111\rangle$ axis of about 0.6 Å.

(A1)

$|0\rangle$

$\left\{\begin{array}{l}\frac{2}{3}^{1/2}|-2\rangle+\frac{1}{3}^{1/2}|1\rangle\\ -\frac{1}{3}^{1/2}|-1\rangle+\frac{2}{3}^{1/2}|2\rangle\end{array}\right.$

$\left\{\begin{array}{l}\frac{1}{3}^{1/2}|-2\rangle-\frac{2}{3}^{1/2}|1\rangle\\ \frac{2}{3}^{1/2}|-1\rangle+\frac{1}{3}^{1/2}|2\rangle\end{array}\right.$

(A2)

$|0\rangle$

$\left\{\begin{array}{l}\frac{2}{3}^{1/2}|-2\rangle+\frac{1}{3}^{1/2}|1\rangle\\ -\frac{1}{3}^{1/2}|-1\rangle+\frac{2}{3}^{1/2}|2\rangle\end{array}\right.$

$\left\{\begin{array}{l}\frac{1}{3}^{1/2}|-2\rangle-\frac{2}{3}^{1/2}|1\rangle\\ \frac{2}{3}^{1/2}|-1\rangle+\frac{1}{3}^{1/2}|2\rangle\end{array}\right.$

(B1)

$\left\{\begin{array}{l}\frac{1}{3}^{1/2}|-2\rangle-\frac{2}{3}^{1/2}|1\rangle\\ \frac{2}{3}^{1/2}|-1\rangle+\frac{1}{3}^{1/2}|2\rangle\end{array}\right.$

$\left\{\begin{array}{l}\frac{2}{3}^{1/2}|-2\rangle+\frac{1}{3}^{1/2}|1\rangle\\ -\frac{1}{3}^{1/2}|-1\rangle+\frac{2}{3}^{1/2}|2\rangle\end{array}\right.$

$|0\rangle$

(B2)

$\left\{\begin{array}{l}\frac{1}{3}^{1/2}|-2\rangle-\frac{2}{3}^{1/2}|1\rangle\\ \frac{2}{3}^{1/2}|-1\rangle+\frac{1}{3}^{1/2}|2\rangle\end{array}\right.$

$\left\{\begin{array}{l}\frac{2}{3}^{1/2}|-2\rangle+\frac{1}{3}^{1/2}|1\rangle\\ -\frac{1}{3}^{1/2}|-1\rangle+\frac{2}{3}^{1/2}|2\rangle\end{array}\right.$

$|0\rangle$

(C1)

$\left\{\begin{array}{l}0.91|-2\rangle+0.43|1\rangle\\ -0.43|-1\rangle+0.91|2\rangle\end{array}\right.$

$|0\rangle$

$\left\{\begin{array}{l}0.43|-2\rangle-0.91|1\rangle\\ 0.91|-1\rangle+0.43|2\rangle\end{array}\right.$

(C2)

$\left\{\begin{array}{l}0.93|-2\rangle+0.36|1\rangle\\ -0.36|-1\rangle+0.93|2\rangle\end{array}\right.$

$\left\{\begin{array}{l}0.36|-2\rangle-0.93|1\rangle\\ 0.93|-1\rangle+0.36|2\rangle\end{array}\right.$

$|0\rangle$

(D1)

$\left\{\begin{array}{l}0.95|-2\rangle+0.31|1\rangle\\ -0.31|-1\rangle+0.95|2\rangle\end{array}\right.$

$\left\{\begin{array}{l}0.31|-2\rangle-0.95|1\rangle\\ 0.95|-1\rangle+0.31|2\rangle\end{array}\right.$

$|0\rangle$

probably, sevenfold-coordinated Zr^{3+}, if they exist in YSZ, may be present in configurations like those of Fig. 1(b) which give rise to a ground state composed by a complex admixture of $|0\rangle$ and Γ_3 states very close in energy to other levels [Table I (25–27)] whose thermal excitation may prevent the EPR observation via spin-lattice relaxation mechanisms.

As a result of the above considerations, it seems more likely, in contrast with our preliminary proposal, that the signal rises from sixfold-coordinated Zr^{3+} ions. Some sort of disorder in the oxygen displacements, compared to the configuration of Fig. 1(c), may be responsible for the observed linewidth anisotropy and signal symmetry.

Finally, our calculations indicate that the crystal-field splittings obtained in the sevenfold-coordinated configurations tend to be smaller than in the sixfold-coordinated ones. This suggests that optical transitions should be correspondingly different for the two types of site. In fact two optical absorptions observed in cubic zirconia, at 375 nm (3.31 eV) and 480 nm (2.58 eV), have been assigned tentatively to sixfold- and sevenfold-coordinated Zr^{3+} ions, respectively, under the assumption that only one of these, the former, possesses an EPR signal.[6] It may now be seen whether this proposed attribution is consistent with the presented crystal-field calculations by comparing the experimental energies of the optical transitions with the cubic field splitting of the sixfold- and sevenfold-coordinated configurations of Figs. 1(b) and 1(c): Indeed, the former gives rise to an axial g tensor consistent with the experimental signal, while the latter may give no EPR signal. From the difference between the mean energies of the lower energy levels and of the higher ones we obtain 3.23 eV for the sixfold-coordinated configuration of Fig. 1(c) and 2.72 eV for the sevenfold-coordinated configuration of Fig. 1(b), in good agreement with the optical data.

ACKNOWLEDGMENTS

This work was carried out within the "Progetto Finalizzato Materiali speciali per Tecnologie Avanzate" research program of the Italian National Research Council (CNR).

[1]C. B. Azzoni and A. Paleari, Solid State Ionics **44**, 267 (1991).
[2]J. S. Thorp, A. Aypar, and J. S. Ross, J. Mater. Sci. **7**, 729 (1972).
[3]K. K. Ermakovich, V. N. Lazukin, I. V. Chepeleva, and V. I. Aleksandrov, Fiz. Tverd. Tela (Leningrad) **18**, 1755 (1976) [Sov. Phys. Solid State **18**, 1022 (1976)].
[4]J. Genossar and D. S. Tannhauser, Solid State Ionics **28-30**, 503 (1988).
[5]C. B. Azzoni and A. Paleari, Phys. Rev. B **40**, 6518 (1989).
[6]V. M. Orera, R. I. Merino, Y. Chen, R. Cases, and P. J. Alonso, Phys. Rev. B **42**, 9782 (1990).
[7]A. Abragam and B. Bleany, *Electron Paramagnetic Resonance of Transition Ions* (Oxford University, New York, 1970), p. 456.
[8]M. Morinaga, H. Adachi, and M. Tsukada, J. Phys. Chem. Solids **44**, 301 (1983).
[9]See, for example, M. T. Hutchings, in *Solid State Physics*, edited by F. Seitz and D. Turnbull (Academic, New York, 1965), Vol. 16, p. 227.
[10]D. Steele and B. E. F. Fender, J. Phys. C. **7**, 1 (1974).
[11]G. R. Asatryan, A. S. Kuzanyan, A. G. Petrosyan, and E. G. Sharoyan, Fiz. Tverd. Tela (Leningrad) **27**, 3441 (1985) [Sov. Phys. Solid State **27**, 2073 (1985)].
[12]Abragam and Bleany (Ref. 7), p. 790.